Inorganic Chemistry

Article

pubs.acs.org/IC

Aerial Oxidation of a V^{IV}–Iminopyridine Hydroquinonate Complex: A Trap for the V^{IV}–Semiquinonate Radical Intermediate

Marios Stylianou,[†] Chryssoula Drouza, [‡] John Giapintzakis,[§] Georgios I. Athanasopoulos,[§] and Anastasios D. Keramidas*[,†]

[†]Department of Chemistry, University of Cyprus, 1678 Nicosia, Cyprus

[‡] Department of Agriculture Production, Biotechnology and Food Science, Cyprus University of Technology, 3036 Limasol, Cyprus

[§]Department of Mechanical and Manufacturing Engineering, University of Cyprus, 1678 Nicosia, Cyprus

Supporting Information

ABSTRACT: The reaction of 2,5-bis[*N*,*N*′-bis(2-pyridylaminomethyl)aminomethyl]-*p*-hydroquinone (H_2bpymah) with VO^{2+} salts in acetonitrile or water at a low pH (2.2–3.5) results in the isolation of $[\{V^{IV}(O)(Cl)\}_2(\mu$-bpymah)], the *p*-semiquinonate complex $[\{V^{IV}(O)(Cl)\}_2(\mu$-bpymas)](OH), the cyclic mixed-valent hexanuclear compound $[\{V^{V}(O)(\mu$-$O)V^{IV}(O)\}(\mu$-bpymah)]$_3$, and $[(V^{V}O_2)_2(\mu$-bpymah)]. $[\{V^{IV}(O)(Cl)\}_2(\mu$-bpymas)](OH) is an intermediate of the radical-mediated oxidation of $[\{V^{IV}(O)(Cl)\}_2(\mu$-bpymah)] from O_2. At lower pH values (2.2), a reversible intramolecular electron transfer from the metal to the ligand of $[\{V^{IV}(O)(Cl)\}_2(\mu$-bpymas)](OH) is induced with the concurrent substitution of chlorine atoms by the oxygen-bridging atoms, resulting in the formation of $[\{V^{V}(O)(\mu$-$O)V^{IV}(O)\}(\mu$-bpymah)]$_3$. The metal complexes were fully characterized by X-ray crystallography, infrared (IR) spectroscopy, and magnetic measurements in the solid state, as well as by conductivity measurements, UV–vis spectroscopy, and electrochemical measurements in solution. The oxidation states of the metal ions and ligands were determined by the crystallographic data. The $[\{V^{IV}(O)(Cl)\}_2(\mu$-bpymah)]–$[\{V^{IV}(O)(Cl)\}_2(\mu$-bpymas)](OH) redox process is electrochemically reversible. The V^{IV} ion in the semiquinonate compound exhibits a surprisingly low oxophilicity, resulting in the stabilization of OH^- counterions at acidic pH values. An investigation of the mechanism of this reaction reveals that these complexes induce the reduction of O_2 to H_2O_2, mimicking the activity of enzymes incorporating two redox-active centers (metal–organic) in the active site.

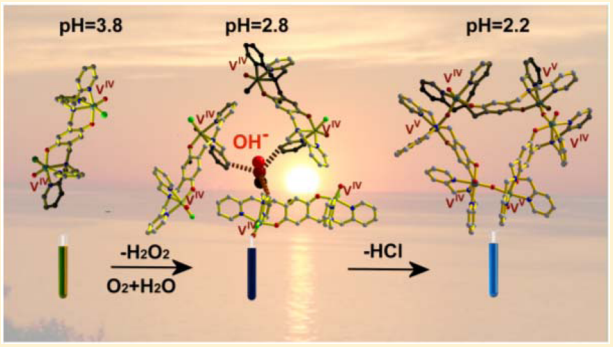

INTRODUCTION

Hydroquinone/*p*-semiquinone and catecholate/*o*-semiquinonate molecular systems play important roles as proton/electron sources and sinks in biological systems.[1−4] The metal ions in these systems lie in close proximity to *p*-semiquinone radicals, resulting in immediate interaction. For example, the proposed catalytic cycle in copper amine oxidases (CAOs) involves the intermediate reduced state of the enzyme containing aminoquinol and a cupric ion in equilibrium with the enzyme form whose proton and electron transfer lead to a cuprous ion–iminosemiquinone pair. Enzymes that exhibit two redox centers, inorganic–organic, such as galactose oxidase and copper amine oxidase, in the active site utilize O_2 to oxidize organic substrates, releasing H_2O_2.[5−9] The design of new compounds that mimic the activity of the two redox center enzymes is of particular interest because of their potential applications.[10−15] For example, the activation of O_2 can be used as a green oxidant and in the facile on-site production of H_2O_2. H_2O_2 is also a powerful green oxidant[16,17] and can be used for clean energy storage.[18,19] These complexes, producers of reactive oxygen species (ROS), are also potential anticancer drugs that induce apoptosis of cancer cells.[20−22]

The vanadium complexes are of particular interest because it has been found that vanadium-based enzymes and complexes catalyze oxidation reactions utilizing O_2 and/or H_2O_2, including oxidative C–H activation, epoxidation, and alcohol oxidation reactions.[23−39] Although O_2 is preferable to other oxidants because of its low cost and high availability, in most of these processes, the reactive peroxides are used in combination with vanadate/peroxovanadate catalysts under strong acidic conditions. Previous studies have shown that certain vanadyl complexes react with O_2, resulting in the respective vanadate/peroxovanadates.[40,41] The strong acidic environment of the catalytic reactions favors reduction of the vanadate catalysts to vanadyl that may reoxidized back to vanadate/peroxovanadates utilizing O_2.[32]

Received: March 12, 2015
Published: July 22, 2015

DOI: 10.1021/acs.inorgchem.5b00571
Inorg. Chem. 2015, 54, 7218–7229

Chart 1. Drawings of the Molecular Structures of Various Disubstituted or Monosubstituted Hydroquinones

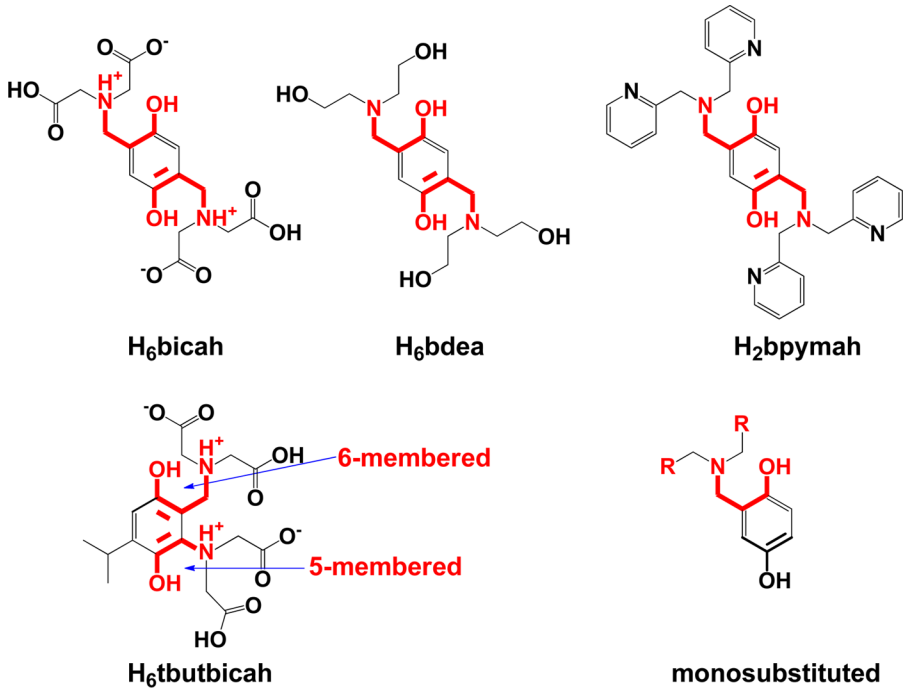

To explore the intrinsic chemistry of the active site of the two redox center (inorganic−organic) enzymes and to mimic and understand their activity over dioxygen activation, we study smaller model complexes. In the past few years, our research team has synthesized stable metal complexes with noninnocent hydroquinonate/*p*-semiquinonate ligands, which model the intermediate states of the radical-mediated reactions of the above biological and catalytic systems.[42−45] The investigation of copper(II) ligation with hydroquinones[46] did not show stabilization of the *p*-semiquinonate radical. The only metal ion found to date to stabilize *p*-semiquinone is vanadium in the oxidation state (IV), thus mimicking the enzymes containing two redox centers in the active site.[43,45,47,48] There is a limited number of stable *p*-(hydro/semi)quinone complexes, mainly because of the absence of a chelate coordination site. A strategy to prepare these species is through the synthesis of substituted *p*-hydroquinones in the ortho position with substituents containing one or more donor atoms, thus enabling the metal atom to form chelate rings. The donor atoms and chelate rings can be varied (Chart 1), regulating the electronic properties of these molecules.[43,45,47,49]

In this study, pyridine donor atoms were selected in the ligand 2,5-bis[*N*,*N*′-bis(2-pyridyl)aminomethyl]-*p*-hydroquinone (H_2bpmah), targeting the stabilization of the vanadium(IV) oxidation state.[50] The V^{IV}−hydroquinonate, [{V^{IV}(O)(Cl)}$_2$(μ-bpymah)], and V^{IV}−semiquinonate, [{V^{IV}(O)(Cl)}$_2$(μ-bpymas)](OH) dinuclear, complexes were isolated and structurally characterized, revealing a ligand-centered reversible redox process in CH_3CN. V^{IV}−hydroquinonate reduces O_2 to H_2O_2 in CH_3CN/H_2O mixtures or to H_2O, resulting in the respective V^{IV}−semiquinonate complex. The positive charge of the V^{IV}−semiquinonate compound is neutralized by hydroxide counteranions, despite the acidic conditions and the excess of chloride anions during complex isolation. UV−vis spectroscopy and X-ray crystallography support that at pH ≈ 2.2, the V^{IV}−semiquinonate species exhibit a slow reversible pH metal to ligand electron transfer toward the formation of the hexanuclear V^{IV}−O−V^{V}-bridged hydroquinonate species.

EXPERIMENTAL SECTION

Materials. Bis(2-methylpyridyl)amine, paraformaldehyde, and sodium vanadate were purchased from Aldrich. All chemicals and solvents were of reagent grade and used without further purification. [$VO(CH_3COO)_2$] and a stock solution of vanadyl chloride 0.920 M were prepared according to the literature.[43,51]

Synthesis of 2,5-Bis[*N*,*N*′-bis(2-pyridyl-aminomethyl)-aminomethyl]-*p*-hydroquinone (H_2bypmah). Bis(2-methylpyridyl)amine (6.00 g, 30.0 mmol) and paraformaldehyde (0.90 g, 30.0 mmol) were added in 25.0 mL of ethyl alcohol. The mixture was heated and stirred to the dissolution of all solids, resulting in the formation of a bright yellow solution. Then hydroquinone (1.66 g, 15.0 mmol) was added, turning the color of the solution to orange. The mixture was refluxed for 8 h, affording a white precipitate. Then it was kept at −15 °C overnight, and a white solid was filtered, washed with acetone, and dried under vacuum. The recrystallization of the product from acetone afforded pale yellow crystals suitable for X-ray diffraction. The yield in H_2bypmah was 60% (4.82 g, 9.00 mmol) based on hydroquinone. Anal. Calcd for $C_{32}H_{32}N_6O_2$: C, 72.16; H, 6.06; N, 15.78. Found: C, 72.15; H, 6.04; N, 15.76. IR (KBr, cm^{-1}): ν(C−$O_{phenolate}$) 1258, ν(py) 1595, 1566. ^{1}H NMR δ(D_2O, ppm): 8.44 (d, J = 5.14 Hz, 4H, H10/py), 8.22 (t, J_1 = 7.87 Hz, J_2 = 8.00 Hz, 4H, H8/py), 7.70 (d, J = 8.58 Hz, 4H, H7/py), 7.66 (t, J_1 = 7.65 Hz, J_2 = 6.37 Hz, 4H, H9/py), 6.08 (s, 2H, H2/hydroquinone), 4.21 (s, 8H, H5/−CH_2), 3.31 (s, 4H, H4/−CH_2). ^{13}C NMR δ(D_2O, ppm): 152.9 (C6/py), 147.6 (C1/hydroquinone), 146.8 (C10/py), 140.6 (C8/py), 126.9 (C7/py), 126.0 (C9/py), 123.5 (C3/hydroquinone), 118.7 (C2/hydroquinone), 57.5 (C5/−CH_2), 55.1 (C4/-CH_2). The numbering is according to Figure 1.

Synthesis of [(V^{IV}O)$_2$(μ-bpymas)(Cl)$_2$](OH)·6H_2O (1·6H_2O). A suspension of H_2bpymah (0.800 g, 1.50 mmol) in acetonitrile (30.0 mL) was dissolved with the addition of triethylamine (0.420 mL, 3.00 mmol) under Ar atmosphere. The solution was heated followed by the addition of vanadyl chloride (3.30 mL of 0.920 M freshly prepared acetonitrile solution, 3.00 mmol), resulting in the formation of a brown precipitate (**2**·2CH_3CN). The precipitate was filtered. The suspension of the brown solid in acetonitrile (30 mL) and H_2O (2

DOI: 10.1021/acs.inorgchem.5b00571
Inorg. Chem. 2015, 54, 7218−7229

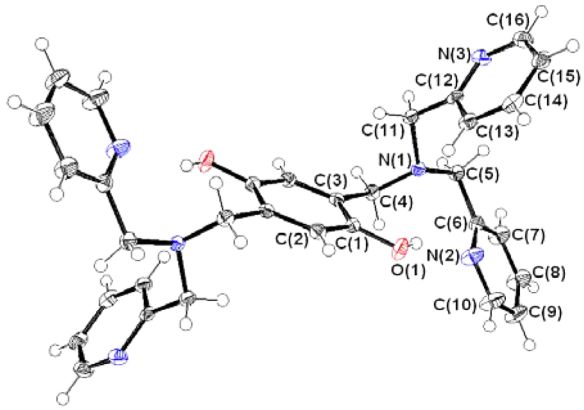

Figure 1. ORTEP drawing of H_2bpymah with atom labels and numbering, at 50% probability ellipsoids.

mL) was refluxed to complete dissolution of the solid (slight acidification of the suspension with HCl accelerates the reaction). The hot dark blue solution was filtered and cooled at room temperature. Dark blue single crystals of **1**·9.5H_2O and **1**·7H_2O suitable for X-ray diffraction analysis were obtained over a period of a week. The crystals were separated by filtration and dried in atmospheric air. The elemental analysis of the solid agrees with the stoichiometry of **1**·6H_2O. The yield in **1**·6H_2O was 67% (0.86 g, 1.0 mmol) based on H_2bpymah. Anal. Calcd for **1**·6H_2O, $C_{32}H_{43}Cl_2N_6O_{11}V_2$: C, 44.66; H, 5.04; N, 9.77. Found: C, 44.61; H, 5.08; N, 9.71. IR (KBr, cm^{-1}): ν(py) 1602, 1566, ν(V═O) 972.

Synthesis of [($V^{IV}O$)$_2$(μ-bpymas)(Cl)$_2$](OH)·6H_2O (1·6H_2O) from Water. H_2bpymah (0.800 g, 1.50 mmol) and vanadyl sulfate (0.33 g, 1.5 mmol) were heated in 20.0 mL of water under Ar, giving a brown mixture. Sodium metavanadate (0.18 g, 1.5 mmol), dissolved in 2.0 mL of hot water, was added, resulting in the formation of a blue-purple solution, (pH = 3.4). The pH was adjusted at 2.8 by the dropwise addition of 6.0 M HCl. All solids were dissolved, resulting in a dark blue solution that was stirred for 1 h. The solution was filtered, and acetone (200 mL) was added in the filtrate. Dark blue crystals of **1**·7.5H_2O suitable for X-ray analysis were obtained upon a period of 2 weeks. The elemental analysis of the solid agrees with the stoichiometry of **1**·6H_2O. The yield in **1**·6H_2O was 36% (0.46 g, 0.53 mmol) based on H_2bypmah. Anal. Calcd for **1**·6H_2O, $C_{32}H_{51}Cl_2N_6O_{15}V_2$: C, 42.21; H, 5.51; N, 9.01. Found: C, 42.36; H, 5.30; N, 9.04. IR (KBr, cm^{-1}): ν(py) 1611, ν(V═O) 973. Compound **1**·6H_2O may also be isolated from an aqueous solution of **2** in water at pH 2.8 open in air with the addition of acetone.

Synthesis of [($V^{IV}O$)$_2$(μ-bpmah)(Cl)$_2$]·2CH_3COCH_3 (2·2CH_3COCH_3) and [($V^{IV}O$)$_2$(μ-bpymah)(Cl)$_2$]·2CH_3CN (2·2CH_3CN). H_2bpymah (0.800 g, 1.50 mmol) was dissolved in 30.0 mL of water by the dropwise addition of HCl (2.0 M), resulting in a pale yellow solution (pH 2.0). Vanadyl acetate (0.560 g, 3.00 mmol) was added to the above solution. The color of the mixture turned from yellow to deep brown (pH = 4.7). The mixture was heated and vigorously stirred for 1 h, giving a deep green solution. The solution was filtered. The pH was adjusted at 3.4 by the addition of HCl (2.0 M), and then acetone was added in an amount twice the volume of the solution. Dark red-brown crystals of **2**·2CH_3COCH_3 suitable for X-ray analysis were obtained within a period of 2 weeks. The crystals were filtered and dried on a filter paper. The yield in **2**·2CH_3COCH_3 was 51% (0.65 g, 0.76 mmol) based on H_2bpymah. The complex **2**·2CH_3CN was synthesized according to the procedure followed in **2**·2CH_3COCH_3 with the exception of the addition of CH_3CN instead of acetone. The yield in **2**·2CH_3CN was 59% (0.72 g, 0.88 mmol) based on H_2bpmah. Anal. Calcd for **2**·2CH_3COCH_3, $C_{38}H_{42}Cl_2N_6O_6V_2$: C, 53.60; H, 4.97; N, 9.87. Found: C, 53.52; H, 5.02; N, 9.84. Anal. Calcd for **2**·2CH_3CN, $C_{36}H_{36}Cl_2N_8O_4V_2$: C, 52.89; H, 4.44; N, 13.71. Found: C, 52.81; H, 4.38; N, 13.74. IR for **2**·2CH_3COCH_3 (KBr, cm^{-1}): ν(C−$O_{phenolate}$) 1212, ν(py) 1610, ν(V═O) 992, 947(sh). IR for **2**·2CH_3CN (KBr, cm^{-1}): ν(C−$O_{phenolate}$) 1212, ν(py) 1612, ν(V═O) 994, 950(sh).

Synthesis of [($V^{V}O$)$_2$(μ-bpymah)] (3). H_2bpymah (0.800 g, 1.50 mmol) and vanadyl acetate (0.560 g, 3.00 mmol) suspension were refluxed in 40.0 mL of methanol for an hour. The color of the mixture turned from gray to dark green within an hour. Potassium perchlorate (0.830 g, 6.00 mmol) was then stepwise added, and the mixture was refluxed for 24 h. The resulting brown solution was filtered, and the filtrate was cooled at room temperature. Slow evaporation of the solution afforded dark brown crystals suitable for X-ray analysis. The crystals were filtered and dried on a filter paper. The yield in **3** was 61% (0.64 g, 0.92 mmol) based on H_2bpymah. Anal. Calcd for **3**, $C_{32}H_{30}N_6O_6V_2$: C, 55.18; H, 4.34; N, 12.07. Found: C, 55.18; H, 4.34; N, 12.06. IR (KBr, cm^{-1}): ν(C−$O_{phenolate}$) 1210, ν(py) 1615, ν(V═O) 953. ^{51}V NMR δ(DMSO-d_6, ppm): −490, −520 (*cis,cis-* and *cis,trans-*V═O isomers).

Synthesis of [{$V^{IV}O$(μ-O)$V^{V}O$}(μ-bpymah)$_3$](Cl)$_3$·42H_2O (4). A solution of vanadyl chloride (1.60 mL of 0.920 M freshly prepared acetonitrile solution, 1.50 mmol) was added to a suspension of H_2bypmah (0.800 g, 1.50 mmol) in 2.0 mL of water under Ar, resulting in the formation of a dark blue mixture. Ammonium metavanadate (0.18 g, 1.5 mmol), dissolved in 5.0 mL of hot water, was added, turning the color of the mixture to purple (pH = 4.2). The pH was adjusted at 2.2 by the dropwise addition of HCl (2.0 M). All solids were dissolved, and the resulted dark blue solution was stirred for 1 h at room temperature and then filtered. Acetone (200 mL) was added in the filtrate, and the final solution was kept for 1 month at −20 °C, resulting in the precipitation of dark blue crystals suitable for X-ray analysis. The crystals were filtered and dried on a filter paper. The yield in **4** was 28% (1.22 g, 0.42 mmol) based on H_2bpymah. Anal. Calcd for **4**, $C_{96}H_{174}N_{18}O_{57}Cl_3V_6$: C, 39.70; H, 6.04; N, 8.68. Found: C, 39.52; H, 5.95; N, 8.71. IR (KBr, cm^{-1}): ν(C−$O_{phenolate}$) 1210, ν(py) 1613, ν(V═O) 965, 947(sh), ν(V−O−V) 860. Compound **4** may also be isolated from aqueous solutions of **1** or **2** in water at pH 2.2.

Instrumentation for CHN Analysis and FT-IR and NMR Spectroscopies. Microanalyses for C, H, and N were performed using a Euro-Vector EA3000 CHN elemental analyzer. FT-IR transmission spectra of the compounds, in KBr pellets, were aquired using a JASCO-460 model spectrophotometer. All NMR samples were prepared from crystalline compounds in D_2O, CD_3CN-d_3, or DMSO-d_6 at room temperature immediately before NMR spectrometric determinations. NMR spectra were recorded on a Bruker Avance 300 spectrometer at 300 MHz for ^{1}H and 78.9 MHz for ^{51}V NMR. A 30° pulse width was applied for both the ^{1}H and the ^{51}V NMR measurements, and the spectra were acquired with 3000 and 30 000 Hz spectral window and 1 and 0.1 s relaxation delay, respectively.

The cw X-band EPR spectra of CH_3CN solutions of **1** at 130 K and at RT were measured on an ELEXSYS E500 Bruker spectrometer at resonance frequency ≈ 9.5 GHz and modulation frequency = 100 MHz. The resonance frequency was accurately measured with solid DPPH (g = 2.0036).

Single X-ray Crystal Structure Analysis. Single-crystal analysis was performed on a Xcalibur Oxford Diffractometer equipped with a Sapphire 3 CCD detector and a 4-cycle Kappa geometry goniometer using an enhanced Mo Kα (λ = 0.71073 Å) X-ray source and graphite radiation monochromator. Analytical absorption correction was applied using CrysAlis RED software. CrysAlis CCD and CrysAlis RED software were used for data collection and data reduction/cell refinement, respectively.[52,53] The structure of the compounds was solved by direct methods and refined by full-matrix least-squares techniques on F^2 by using SHELXS-97.[54,55] Special computing molecular graphics incorporated in the WinGX 3.2 interface were used.[56] All non-H atoms were anisotropically refined. The positions of hydrogen atoms in all structures were calculated from stereochemical considerations and kept fixed isotropic during refinement or found in a DF map and refined with isotropic thermal parameters.

Magnetic Measurements. Room-temperature magnetic measurements were carried out on an MK1MB magnetic susceptibility balance. Variable-temperature dc magnetic susceptibility data were collected on

DOI: 10.1021/acs.inorgchem.5b00571
Inorg. Chem. 2015, 54, 7218−7229

powdered samples of complexes **1** and **2** in a 50 kG applied magnetic field and in the temperature range 1.9−300 K using an extraction magnetometer (PPMS-Quantum Design). Magnetization measurements were carried out at various temperatures from 2 to 10 K and in the field range 0−60 kG. Variable-temperature ac magnetization (M′, M″) data were collected in the temperature range from 2 to 300 K using an ac magnetic field of 10 Oe and various frequencies in the range 111−911 Hz.

Electrochemical Measurements. Cyclic voltammetry (CV) and round disk voltammetry (RDV) experiments were recorded using an EG&G Princeton Applied Research 273A potentiostat/galvanostat. Electrochemical procedures were performed with a three-electrode configuration: a platinum disk or rotating disk electrode (RDE) as the working electrode, a platinum wire as the auxiliary electrode, and a platinum wire as a reference. All potential values are referred to NHE using ferrocene as internal reference (0.63 V vs NHE). The electrochemical measurements were carried out in acetonitrile solutions of But_4NClO_4 (0.1 M) purged with N_2 prior to the measurement at 298 K. Scan rates (ν) of 100 and 10 mV s^{-1} were used for cyclic voltammograms and linear sweep voltammetry experiments, respectively. The working electrode was cleaned after every run because depositions on the surface of the electrodes alter the peaks in the voltammograms.

Determination of Chloride Ion Concentration by Titration and Molecular Conductivity Measurements. Volhard's titration method was carried out in order to determine the concentration of chloride ions in solutions of **1** and **2**.

Molecular conductivity measurements were performed using a Jenway 4020 conductivity meter calibrated at 298 K with a commercial standard calibration solution (298 K, 12.88 mS/cm) purchased by NIST. *K* conductivity constant was estimated using 0.0200 M KCl standard solution (k = 0.002768 Ohm^{-1}). All conductivity measurements refer to molar concentrations of complexes 10^{-3} M at 298 K.

UV−vis Kinetic Measurements. The kinetic UV−vis measurements were recorded on a Photonics UV−vis spectrophotometer model 400, equipped with a CCD array, operating in the range from 250 to 1000 nm. Single crystals of **1** (1.15 mM) were dissolved in 0.10 M KCl at 298 K in order to keep the ionic strength constant, and pH was adjusted at 2.14. UV−vis spectra were recorded vs time at time intervals of 1 min.

O_2 Reduction Experiments—Measurements of H_2O_2. The produced H_2O_2 from the oxidation of **2** by O_2 was measured by ^{51}V NMR spectroscopy as monoperoxo- or diperoxovanadate species. A stock solution of vanadium(IV)−hydroquinonate complex **2** (25.0 mM) was prepared by dissolving single crystals of the compound in deuterium oxide, and pD was adjusted at 3.41. The experimental procedures for the O_2 reduction experiments are as follows.

(1) A 250 μL amount of the stock solution of **2** and 0.5 mol equiv of sodium metavanadate (stock solution 167 mM, pD 8.50) were transferred in an NMR tube. The pD of the solution was adjusted at 2.80 by slow addition of dilute deuterium chloride, and D_2O was added up to a 500 μL total volume. Immediately after the pH adjustment, air was bubbled through the solution for 10 min.

(2) A 250 μL amount of the stock solution of **2** and 0.5 mol equiv of $VOCl_2$ (stock solution 0.517 M in CH_3CN) were transferred in an NMR tube. The pD of the solution was adjusted at 2.92 by slow addition of dilute deuterium chloride, and D_2O was added up to a 500 μL total volume. Immediately after the pH adjustment, air was bubbled through the solution for 10 min.

(3) A different sample preparation route was followed in order to investigate the peroxide species formation in CD_3CN solution. $VOCl_2$ (9.70 μL, 10.0 mm final concentration, from stock solution 0.517 M in CH_3CN) and 0.5 mL CD_3CN were transferred in an NMR tube. Dioxygen was bubbled through the solution over a period of 10 min followed by the addition of solid **2** (8.20 mg, 20.0 mM final concentration of **2**). A small quantity of H_2O was added until complete dissolution of solids. The resulted deep blue-colored solution was bubbled with dioxygen for an additional 10 min.

Blank samples were prepared following the same procedures without the addition of complex **2**. The ^{51}V NMR spectrum was acquired immediately after preparation of the solutions.

RESULTS AND DISCUSSION

Syntheses of the Compounds. The hydroquinone ligand H_2bpymah was synthesized using the Mannich reaction. The ligand was characterized by elemental analysis, ^1H NMR, and X-ray crystallography (Figure 1). In this synthesis, 1 equiv of hydroquinone, 2 equiv of formaldehyde, and 2 equiv of bis(2-methylpyridyl)amine were allowed to react in ethanol. Only the bisubstituted hydroquinone in the 2 and 5 positions was obtained.

The syntheses of the vanadium complexes are summarized in Scheme 1. $VOCl_2$, $VO(CH_3COO)_2$, and $VOSO_4$ were used as

Scheme 1. Synthetic Routes for Complexes 1−4

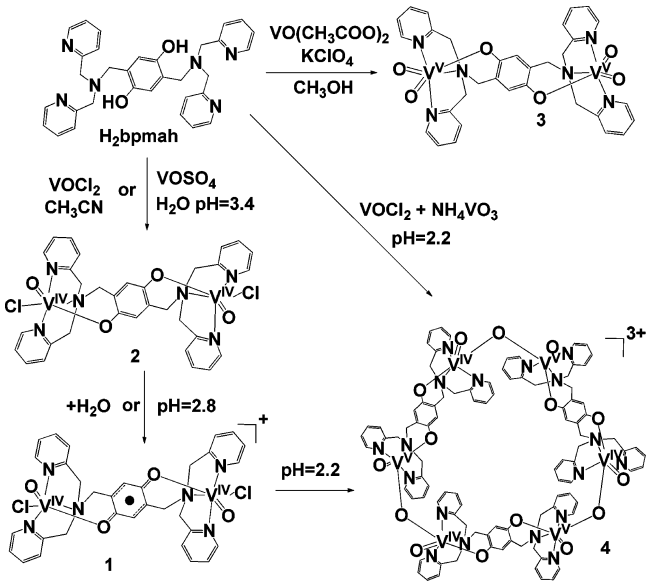

V^{IV} sources for the synthesis of the complexes. To pursue the oxidation of the hydroquinone ligand to semiquinone, in some cases, equimolar mixtures of $VOCl_2$ and $NaVO_3$ were used. However, the type of products is independent of the starting material and determined exclusively by the solvent and the pH of the solution. Binuclear species V^{IV}−hydroquinonate (**2**) and V^{IV}−semiquinonate (**1**) were isolated at pH 3.4 and 2.8, respectively, and the cyclic hexanuclear species (**4**) was isolated at pH 2.2. V^{IV}−hydroquinonate (**2**) was also isolated from acetonitrile solutions. The addition of few drops of water in the open to air vessel results in the oxidation of **2** to **1**. The molecular structures of the binuclear semiquinonate species (**1**) isolated from aqueous solutions at pH 2.8 and from acetonitrile are the same; however, the solvation in the crystal is different (see below for crystallographic characterization).

X-ray Crystallography. The molecular structures of the anions of **1**−**4** are shown in Scheme 1. Crystallographic data are provided in Table 1. Tables 2, 3, and S1−S4, Supporting Information, contain the interatomic bond lengths and angles of **1**−**4**. The vanadium(IV) complexes **1** and **2** (Figure 2A) and vanadium(V) complex **3** (Figure 2B) are dinuclear. The two vanadium centers are bridged together through a μ-hydroquinonate group for **2** and **3** and through a μ-semiquinonate group for **1**. Complex **4** (Figure 3) consists of three dinuclear

DOI: 10.1021/acs.inorgchem.5b00571
Inorg. Chem. 2015, 54, 7218−7229

Table 1. Crystal Data and Structure Refinement for H_2pbymah and Complexes 1−4[a,b]

parameters	H_2pbymah	**1**·9.5H_2O	**1**·7H_2O[c]	**2**·2CH_3COCH_3
empirical formula	$C_{32}H_{32}N_6O_2$	$C_{32}H_{50.2}Cl_2N_6O_{14.6}V_2$	$C_{32}H_{45.6}Cl_2N_6O_{12.3}V_2$	$C_{38}H_{42}Cl_2N_6O_6V_2$
cryst size (mm)	0.17 × 0.12 × 0.07	0.43 × 0.21 × 0.10	0.40 × 0.22 × 0.10	0.25 × 0.14 × 0.08
fw	532.64	925.07	884.12	851.56
cryst syst	triclinic	trigonal	trigonal	monoclinic
space group	$P-1$	$R-3$	$R-3$	$P2_1/c$
a (Å)	8.5184(5)	24.9994(5)	24.9734(4)	6.6604(7)
b (Å)	8.8638(4)	24.9994(5)	24.9734(4)	15.313(2)
c (Å)	9.6279(5)	17.3225(4)	17.3106(5)	18.687(2)
α (deg)	85.629(4)	90.00	90.00	90.00
β (deg)	75.918(5)	90.00	90.00	94.365(8)
γ (deg)	80.203(4)	120.00	120.00	90.00
vol. (Å^3)	694.37(6)	9375.6(3)	9349.7(4)	1900.4(3)
Z	1	9	9	2
ρ_{calcd} (g/cm^3)	1.274	1.475	1.413	1.488
abs coeff (mm^{-1})	0.082	0.648	0.642	0.687
$F(000)$	282	4326	4102	880
θ range for data collection (deg)	3.14−31.16	3.01−34.87	3.26−31.10	3.34−34.81
index ranges	$-11 \le h \le 11$	$-39 \le h \le 37$	$-35 \le h \le 35$	$-10 \le h \le 8$
	$-12 \le k \le 12$	$-39 \le k \le 39$	$-35 \le k \le 36$	$-23 \le k \le 21$
	$-13 \le l \le 13$	$-27 \le l \le 26$	$-24 \le l \le 22$	$-29 \le l \le 27$
no. of reflns collected/unique	15 235/3982	61 155/8389	45 044/6085	34 224/7518
R_{int}	0.0302	0.0729	0.0361	0.0499
data/params	3892/181	8389/263	6085/260	7518/244
GOF on F^2	1.029	0.928	0.999	0.934
max/min Δp (e Å^{-3})	0.357/−0.185	1.963/−1.192	1.318/-0.496	1.623/−0.297
final R/Rw indices [$I > 2\sigma(I)$]	0.0404/0.1031	0.0641/0.1731	0.0542/0.1565	0.0460/0.1211
final R/Rw indices (all data)	0.0609/0.1074	0.1286/0.1935	0.0805/0.1697	0.0947/0.1262
parameters	**2**·2CH_3CN	**1**·7.5H_2O	**3**	**4**
empirical formula	$C_{36}H_{36}Cl_2N_8O_4V_2$	$C_{32}H_{45.89}Cl_2N_6O_{12.45}V_2$	$C_{32}H_{30}N_6O_6V_2$	$C_{96}H_{174}Cl_3N_{18}O_{57.25}V_6$
cryst size (mm)	0.21 × 0.10 × 0.07	0.32 × 0.16 × 0.08	0.15 × 0.10 × 0.06	0.15 × 0.07 × 0.05
fw	817.51	884.60	696.50	2908.51[d]
cryst syst	monoclinic	trigonal	triclinic	monoclinic
space group	$P2_1/c$	$R-3$	$P-1$	$C2_1/c$
a (Å)	6.6738(2)	24.974(1)	6.5655(9)	25.642(2)
b (Å)	15.1821(5)	24.974(1)	10.081(1)	33.986(2)
c (Å)	18.6301(7)	17.5048(6)	11.778(1)	30.352(2)
α (deg)	90.00	90.00	97.64(1)	90.00
β (deg)	95.239(4)	90.00	101.98(1)	105.348(6)
γ (deg)	90.00	120.00	102.25(1)	90.00
vol. (Å^3)	1879.8(1)	9455.0(7)	732.32(2)	25508(3)
Z	2	9	1	8
ρ_{calcd} (g/cm^3)	1.444	1.398	1.579	1.515
abs coeff (mm^{-1})	0.689	0.635	0.696	0.585
$F(000)$	840	4117	358	12184
θ range for data collection (deg)	3.35−31.09	3.26−31.25	3.68−34.75	3.14−27.63
index ranges	$-9 \le h \le 9$	$-35 \le h \le 34$	$-9 \le h \le 9$	$-33 \le h \le 30$
	$-21 \le k \le 21$	$-35 \le k \le 36$	$-14 \le k \le 15$	$-42 \le k \le 42$
	$-25 \le l \le 26$	$-23 \le l \le 25$	$-18 \le l \le 16$	$-38 \le l \le 38$
no. of reflns collected/unique	26 632/5442	42 805/6055	9306/4414	71 728/26 345
R_{int}	0.0935	0.0171	0.0671	0.1215
data/params	5442/235	6055/258	4414/208	26345/1946
GOF on F^2	0.833	1.069	1.060	0.922
max/min Δp (e Å^{-3})	1.050/−0.397	1.363/−0.565	1.202/−1.178	0.682/-0.526
final R/Rw indices [$I > 2\sigma(I)$]	0.0626/0.1246	0.0521/0.1489	0.0787/0.1998	0.0984/0.2129
final R/Rw indices (all data)	0.1565/0.1458	0.0601/0.1563	0.1187/0.2325	0.2552/0.2636

[a]All structures determined at T = 100 K using Mo Kα radiation (λ = 0.71073 Å). [b]Refinement method, full−matrix least−squares on F^2. [c]This structure was determined at T = 89 K. [d]The molecular weight used in the structure, due to the disorder of the solvent molecules, was the one calculated from elemental analysis.

DOI: 10.1021/acs.inorgchem.5b00571
Inorg. Chem. 2015, 54, 7218−7229

Table 2. Selected Bond Lengths (Angstroms) for 1−3

	1·9.5H_2O	1·7H_2O	1·7.5H_2O
V(1)−O(1)	1.911(2)	1.912(2)	1.912(1)
V(1)−O(2)	1.603(2)	1.606(2)	1.604(2)
V(1)−Cl(1)	2.323(1)	2.325(1)	2.339(1)
V(1)−N(1)	2.301(2)	2.305(2)	2.306(2)
V(1)−N(2)	2.132(2)	2.133(2)	2.130(2)
V(1)−N(3)	2.105(2)	2.107(2)	2.109(2)

	2·2$(CH_3)_2CO$	2·2CH_3CN	3	
V(1)−O(1)	1.941(1)	1.938(2)	V(1)−O(1)	1.903(2)
V(1)−O(2)	1.606(2)	1.613(2)	V(1)−O(2)	1.630(3)
V(1)−Cl(1)	2.3701(6)	2.374(1)	V(1)−O(3)	1.645(3)
V(1)−N(1)	2.284(2)	2.291(3)	V(1)−N(1)	2.297(3)
V(1)−N(2)	2.137(2)	2.129(3)	V(1)−N(2)	2.317(3)
V(1)−N(3)	2.159(2)	2.156(3)	V(1)−N(3)	2.157(3)

Table 3. Selected Bond Lengths (Angstroms) for 4

V(IV)−O(2)	1.588(5)	1.585(5)	1.568(6)
V(IV)−O(3)	1.847(5)	1.904(5)	1.905(5)
V(IV)−O(1)	1.914(4)	1.919(5)	1.924(6)
V(IV)−N(3)	2.121(6)	2.118(5)	2.122(8)
V(IV)−N(2)	2.150(6)	2.153(6)	2.137(9)
V(IV)−N(1)	2.258(5)	2.257(6)	2.274(6)
V(V)−O(2)	1.584(5)	1.606(5)	1.602(6)
V(V)−O(3)	1.772(5)	1.722(5)	1.718(5)
V(V)−O(1)	1.850(5)	1.850(5)	1.845(5)
V(V)−N(3)	2.136(6)	2.141(6)	2.136(7)
V(V)−N(2)	2.196(6)	2.195(6)	2.195(8)
V(V)−N(1)	2.266(6)	2.286(6)	2.269(7)

hydroquinonate−$V^{IV/V}$ units bridged to each other with V^{IV}−O−V^{V} bonds, occupying the sides of an equilateral triangle (~9.6 Å length of each side of the triangle defined by the three bridging oxygen atoms).

The coordination environment around each vanadium atom in **1**−**4** is octahedral with one oxo group and the amine nitrogen atom of the tripod ligating group occupying the apical positions. The oxygen atom and the two nitrogen atoms originated from the hydroquinonate or semiquinonate, and the two pyridines of the tripod moiety occupy three out of the four equatorial positions of the octahedron. The fourth equatorial position is occupied by a chlorine atom in complexes **1** and **2**, an oxo group in **3**, and the bridging oxo group in complex **4**. The V−$N_{pyridine}$ bond distances range from 2.11 to 2.16 Å, except for the V−$N_{pyridine}$ bond distance of the pyridine trans to the oxo group in complex **3**, which is longer [2.317(3) Å] due to the strong trans effect of the oxo group. The trans effect also causes lengthening of the V−N_{amine} lying on the equatorial plane (2.28 Å; average bond length) in all complexes.

The bond distances between the vanadium ions and the donor atoms provide an infallible tool for distinguishing the oxidation state of vanadium ions in its complexes. One method to determine the oxidation state is to use the bond valence (BVS) calculations, which result in the oxidation state of the metal ion considering the sums of all the metal−donor atoms bond distances. The oxidation states of the vanadium ions in all crystal structures using the BVS were calculated, and the results are summarized in Table 4. One interesting feature of the crystal structure of **4** is the V^{V}−$O_{hydroquinonate}$ and V^{V}−$O_{bridged}$

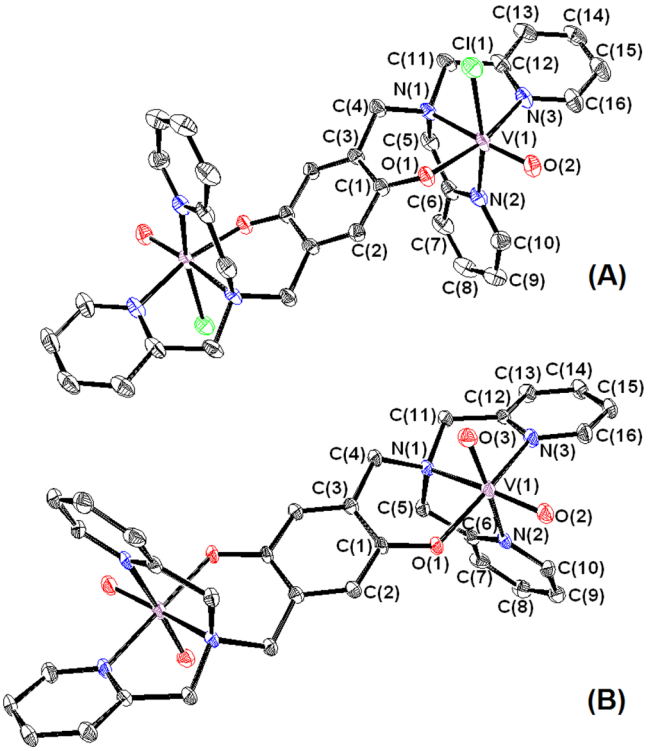

Figure 2. ORTEP drawings and atom labels of the binuclear complexes **1** (A) and **3** (B). The structures of V^{IV}−hydroquinonate/semiquinonate dinuclear units of **1** and **2** complexes are similar. Hydrogen atoms and cocrystallized ions/molecules are omitted for clarity. Ellipsoids are drawn at the 50% probability level.

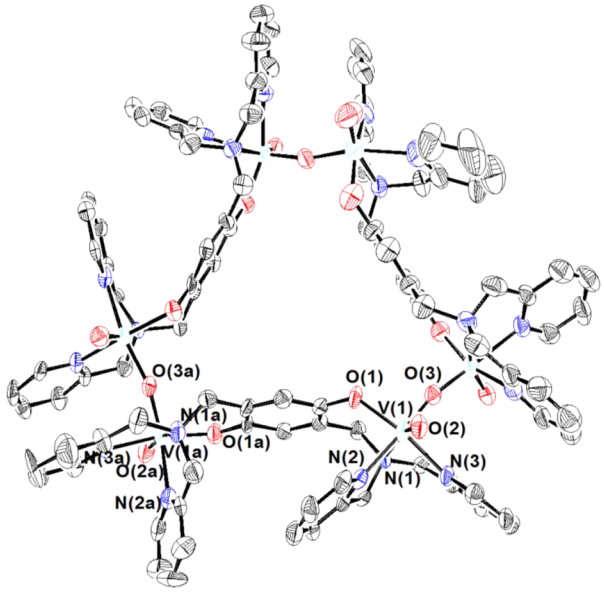

Figure 3. ORTEP drawing of the hexanuclear $V^{IV/V}$−hydroquinonate complex **4** at 50% probability ellipsoids with atom-labeling scheme. Hydrogen atoms and ions/water cocrystallized molecules are omitted for clarity.

bond lengths, which are shorter [from 1.846(5) to 1.852(5) and 1.714(5) to 1.769(5) Å, respectively] than the respective V^{IV} bond lengths [from 1.912(4) to 1.923(6) and 1.850(5) to 1.909(5) Å, respectively], indicating that the spins in this mixed-valent complex are localized. These localized structures have been observed for dinuclear mixed-valent V^{V}/V^{IV} species

DOI: 10.1021/acs.inorgchem.5b00571
Inorg. Chem. 2015, 54, 7218−7229

Table 4. Comparison of Selected Chemical Bonds (Angstroms), Δ Statistical Analysis, and Bond Valence Sums Calculations for Complexes 1−4

compound	V=O (Å)	V−$O_{HQ/Q}$ (Å)	V−$O_{bridged}$ or V=$O_{terminal}$ (Å)	C−$O_{HQ/Q}$ (Å)	Δ	BVS ($V^{IV/V}$)
H_2bpymah				1.366(1)	−1.88, HQ	
1·9.5H_2O	1.603(2)	1.911(2)		1.300(3)	−0.92, SQ	+4.14 (V^{IV})
1·7H_2O	1.604(2)	1.912(2)		1.297(2)	−0.92, SQ	+4.10 (V^{IV})
2·2CH_3COCH_3	1.606(2)	1.941(1)		1.329(2)	−1.67, HQ	+3.92 (V^{IV})
2·2CH_3CN	1.613(2)	1.938(2)		1.345(4)	−1.77, HQ	+3.90 (V^{IV})
1·7.5H_2O from water	1.604(2)	1.912(2)		1.301(2)	−1.12, SQ	+4.08 (V^{IV})
3	1.645(3)	1.903(2)	1.630(3)	1.345(4)	−1.61, HQ	+4.98 (V^{V})
4	1.588(5)	1.914(4)	1.847(5)	1.332(7)	−1.65, HQ	+4.36 (V^{IV})
	1.606(5)	1.850(5)	1.722(5)	1.325(8)		+5.17 (V^{V})
	1.585(5)	1.919(5)	1.904(5)	1.347(8)	−1.91, HQ	+4.24 (V^{IV})
	1.584(5)	1.850(5)	1.772(5)	1.343(8)		+5.03 (V^{V})
	1.568(6)	1.924(6)	1.905(5)	1.349(9)	−1.82, HQ	+4.35 (V^{IV})
	1.602(6)	1.845(5)	1.718(5)	1.345(7)		+5.03 (V^{V})

containing an asymmetric bent V−O−V bridge (angle less than 160°) and one or two π-donor ligands at the equatorial *xy* plane (the short terminal V=O bond defines the *z* axis).[57−63] However, σ-donor atoms at the equatorial plane result in the formation of mixed-valent V^V/V^{IV} complexes with delocalized valences containing symmetric and linear V−O−V bridges.[64−69] The hexanuclear complex **4** has V−O−V angles larger than 160° (∼166°), even though the valences are localized at the vanadium centers. Presumably, steric interactions in the triangular structure do not permit further bending of the V−O−V bridges.

The oxidation state of the *p*- and *o*-dioxolene ligands can be reasonably established by examination of the C−$O_{phenolate}$ and the C−$C_{aromatic}$ bond lengths, which are strongly dependent on the formal charge of the ligands.[42,43,70−73] $d_{C-Ohydroquinonate}$ ranges from 1.329(2) to 1.366(1) Å for **2**, **3**, and **4** is typical for the hydroquinonate complexes.[74−79] The shorter $d_{C-Osemiquinonate}$ [1.297(2)−1.301(2) Å] lengths in complex **1** reveal the semiquinone oxidation state of the ligand. The oxidation state of the ligand was also calculated from eqs 1 and 2 (Δ = 0, −1, and −2 ideal values for quinone, semiquinonate, and hydroquinonate, respectively),[42,43,80] where d_i is the *i*th bond length of the dioxolene moiety under examination, d_{1i} and d_{2i} are the *i*th bond lengths of the uncomplexed hydroquinone and *p*-quinone molecules,[81−87] respectively, and *n* is the number of the dioxolene bonds.

$$\Delta_i = -2(d_i - d_{2i})/(d_{1i} - d_{2i}) \quad (1)$$

$$\Delta = (\sum \Delta_i)/n \quad (2)$$

The results from the application of Δ statistical analysis on complexes **1**−**4** confirmed the oxidation state of the organic redox centers (Table 4).

One of the most interesting features in the structure of these complexes is the variation of the $V^{IV/V}$−$O_{hydroquinonate/semiquinonate}$ bond distances, which is dependent on the oxidation states of the metal ion and the ligand (Table 4). More specifically, V^V−$O_{hydroquinonate}$ [1.903(2) Å in complex **3**] is shorter than V^{IV}−$O_{semiquinonate}$ [∼1.912 Å for complex **1**]. However, the V^{IV}−$O_{hydroquinonate}$ bond lengths [1.941(1) and 1.938(2) Å for complexes **2**] are significantly longer. These data show that V^{IV} exhibits a higher affinity for the semiquinonate than for the hydroquinonate oxygen donor atom, in agreement with previous results for the $V^{IV/V}$−{2,5-bis[*N*,*N*-bis(carboxymethyl)aminomethyl]semiquinonate/hydroquinonate} (bicas^{5-}/bicah^{6-}) complexes.[43] More information about the affinity of the V^{IV} ion for the semiquinonate oxygen is being obtained from the C−$O_{hydroquinonate/semiquinonate}$−V angle. In the dinuclear species, the C−$O_{semiquinonate}$−V^{IV} angles [∼135.3°] are measured to be larger than the angles of C−$O_{hydroquinonate}$−V^V [131.6(2)°] and C−$O_{hydroquinonate}$−V^{IV} [126.8(1) and 127.5(2)°], indicating that the V^{IV}−$O_{semiquinonate}$ bond has significant π character.[48,88] The C−$O_{hydroquinonate}$−V^{IV} angles [128.4(7)°, 127.2(6)°, and 126(3)°] of **4** are close to the values observed for the respective angles in the V^{IV} dinuclear species. However, the C−$O_{hydroquinonate}$−V^V angles (∼135°) of the hexanuclear complex are significantly larger (better π overlap) than the respective angles (131.6°) of the dinuclear species, **3**. This is attributed to the π antagonism between the $O_{hydroquinonate}$ and the bridged oxo group in **4** and between the $O_{hydroquinonate}$ and the terminal oxo group in **3**. The C−$O_{hydroquinonate}$−V^V angle is inversely regulated by the π-donating properties of the remainder of the ligated atoms (the terminal oxo group is a stronger π donor than the bridged oxo group).

In addition, the coordinating angle between the pyridine nitrogen donors and the vanadium atom, N(2)−V(1)−N(3), is much smaller for the V(V)−hydroquinonate (∼75° for complexes **3** and **4**) than for the V(IV)−semiquinonate (∼89° for complex **1**) and V(IV)−hydroquinonate (∼94° for complexes **2** and **4**), resulting in the different orientation of the pyridine rings, syn and anti for V(IV) and V(V), respectively (Figures 2 and 3). This is also attributed to the competition of π-bonding orbitals for the metal, which is much more extended for V(V) (d^0) than V(IV) (d^1). The small N(2)−V(1)−N(3) angle reduces the overlap between the pyridine nitrogen and the metal orbitals. In the absence of competition between the nitrogen atoms for the d orbitals due to the small overlap, the oxo and hydroquinonate oxygen atoms monopolize the vanadium(V) d orbitals for the formation of π bonds.

The total charge of the dinuclear and hexanuclear complexes calculated by counting the charges of the metal ions and the ligands reveals that complexes **2** and **3** are neutral, whereas **1** and **4** are positively charged. In contrast to the neutral complexes, the dinuclear semiquinonate cations in their structures are surrounded by oxygen atoms assigned to water molecules and hydroxide counterions. To confirm this, in addition to C, H, N analysis, the compounds were analyzed for Cl^- and the number of ions in solution was calculated from the molecular conductivity of the complexes in strong donating solvents, such as DMSO, DMF, and H_2O, and weak donating

DOI: 10.1021/acs.inorgchem.5b00571
Inorg. Chem. 2015, 54, 7218−7229

solvents, such as CH_3CN (Table S5, Supporting Information). The Cl^- analysis and the conductivity measurements showed that complexes **1** do not contain additional ionic chlorine but are 1:1 salts, as expected. The presence of the hydroxide counterions is surprising considering that both of the complexes were isolated under acidic conditions from aqueous and acetonitrile solutions in the presence of excess of Cl^-.

In the crystal structures of **1**, three dinuclear vanadium species are arranged in a triangular formation [Figure 4, the

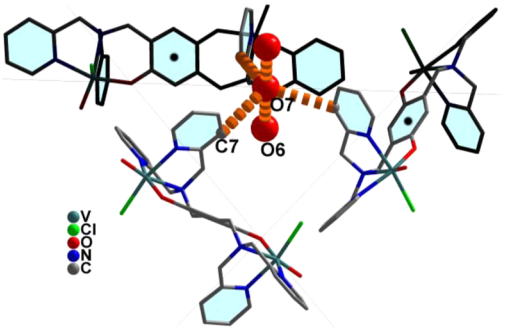

Figure 4. Stick diagram of the crystal structure of **1**·$7H_2O$ showing the three hydroxides interacting with three dinuclear vanadium(IV) semiquinonate units. Dashed orange thick lines show the hydrogen bonds between the hydroxides [O(6)−O(7), 2.640(7) Å] and the interaction of hydroxides with neighboring pyridine rings [C(7)−H---O(7), 3.508(4) Å]. The three dinuclear vanadium species form a triangle defined from the three semiquinonate oxygen atoms O(1) [13.449(4) Å each side].

length {13.449(4) Å} for each side of the triangle is defined by the three semiquinonate oxygen atoms O(1)]. In the middle of the two triangles, three hydroxides are located on a line perpendicular to the two layers and parallel to axis *c*. The three hydroxides are connected to each other through strong hydrogen bonds [O(6)−O(7), 2.605(7) Å] in **1**·$9.5H_2O$. The distance between the hydroxide counterions O(6)−O(7) in **1**·$7H_2O$ and **1**·$7.5H_2O$ are 2.640(7) and 2.736(8) Å, respectively.

The linear arrangements of the hydrogen-bonded O(6)−O(7)−O(6) in structures of **1** are highly similar to the position of the hydroxides in the crystal structures of the alkaline earth hydroxides, thus further confirming our assignments for O(6) and O(7) as hydroxides. For example, in the structure of $Sr(OH)_2·8(H_2O)$, the hydroxides have a similar linear hydrogen-bonded arrangement (OH---OH, 2.845 Å).[89]

In addition to the strong hydrogen bonds between the hydroxides and the ionic interactions between the OH^- and the $[(V^{IV}O)_2(\mu\text{-bpymas})(Cl)_2]^+$, the $d_{O(7)\cdots C(7)} \approx 3.51$ Å between the OH^- and the pyridine carbon atoms of the three surrounding dinuclear species shows the presence of weak C−H---O hydrogen bonds that may also contribute to OH^- stabilization.

Magnetic Measurements and EPR and NMR Spectroscopies. At 298 K, complexes **1**, **2**, and **4** have effective magnetic moments of 2.42, 2.45, and 3.46 μ_B, respectively, which is less than the predicted spin-only values for two and three noninteracting one-electron paramagnetic centers (3.00 and 4.24 μ_B). The reduced magnetic moments in these complexes indicate an antiferromagnetic exchange interaction between the paramagnetic centers.

The temperature dependence of χ_M for complexes **1** and **2** is shown in Figure 5. The data were fit to the Curie−Weiss law

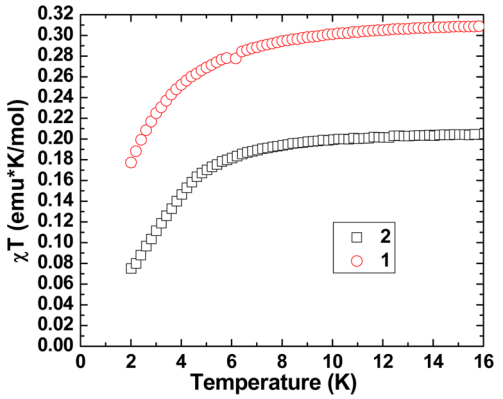

Figure 5. Diagram of χT vs T of complexes **1** and **2**. Data were fit to the Curie−Weiss law (eq 1) in the temperature ranges 2−300 and 10−300 K for complexes **1** and **2**, respectively.

(eq 3) in the temperature ranges 2−300 and 10−300 K for complexes **1** and **2**, respectively, as follows

$$\chi = \chi_0 + \frac{C}{T - \Theta} \quad (3)$$

where χ_0 is the temperature-independent susceptibility, C is the Curie constant, and Θ is the Curie temperature. Satisfactory fitting was obtained with $\chi_0 = -8.8 \pm 0.3 \times 10^{-4}$ emu/mol, C = 0.373 ± 0.001 emu-K/mol, and $\Theta = -1.99 \pm 0.02$ K for complex **1** and $\chi_0 = -1.93 \pm 0.04 \times 10^{-4}$ emu/mol, C = 0.221 ± 0.001 emu-K/mol, and $\Theta = -1.00 \pm 0.03$ K for complex **2**. The C value for complex **1** corresponds to a paramagnetic ensemble of spins with $S = 1/2$ and $g = 2.00$. This indicates that the free radical couples antiferromagnetically to one of the V(IV) d^1 spins. The C value of complex **2** corresponds to a paramagnetic ensemble of spins with $S = 1/2$ and $g = 1.53$. The reduced g value indicates a strong spin−orbit coupling between the V(IV) d^1 spins. The negative Θ values indicate the existence of weak antiferromagnetic interactions.

The $\chi_M(T)$ for complex **2** exhibits a plateau-like behavior below T = 4.5 K. In addition, the M vs H curve at T = 2 K (shown in Figure S1, Supporting Information) for complex **2** exhibits a hysteresis at intermediate magnetic fields but shows zero hysteresis at H = 0. This behavior is characteristic of systems with coexisting strong antiferromagnetic and ferromagnetic interactions. This is corroborated by an anomaly occurring at 3.5 K in the ac susceptibility data $M'(T)$ for various frequencies, indicative of a magnetic phase transition.

The magnetic studies of **1** and **2** showed that the two complexes are magnetically distinct. Complex **1** displays Curie−Weiss paramagnetic behavior over the entire investigated temperature range due to antiferromagnetic coupling between the free radical and one of the d^1 metal ions. Complex **2** displays Curie−Weiss paramagnetic behavior in the temperature range from 10 to 300 K and strong ferromagnetic and antiferromagnetic interactions between the two d^1 metal ions at temperatures lower than 3.5 K.

The CH_3CN solution of **1** at room temperature was silent at the X-band EPR and gave a broad unresolved peak at g = 1.970 at 130 K (Figure S2, Supporting Information). This is typical for spectra of the multinuclear V(IV)−semiquinonate complexes due to the strong exchange and dipolar electron−electron interactions.[41]

Complex **3** is diamagnetic, and its ^{51}V NMR spectra in DMSO-d_6 gave two peaks at −490 and −520 ppm. The two

DOI: 10.1021/acs.inorgchem.5b00571
Inorg. Chem. 2015, 54, 7218−7229

peaks based on ^{1}H NMR were assigned to the two isomers having the four oxo groups on the two vanadium atoms in anti,anti and syn,anti positions (Figure S3, Supporting Information).[90] ^{1}H NMR spectra gave broad peaks, indicating a fast intramolecular exchange.

UV−vis Spectroscopy and pH-Induced Intramolecular Electron Transfer. The UV−vis absorbance data for the semiquinonate compound **1** in CH_3CN are collected in Table 5. The V^{IV} d−d transitions of the semiquinonate complex **1** are

Table 5. UV−vis Data of Semiquinonate Vanadium(IV) Complex 1 in (CH_3CN, 25°C)

λ_{max} (nm)	ε (M cm^{-1}), LMCT
788	11 792
700sh	5720
592	2809
468	1730
388sh	3056
318	6918

overlapped by a strong (ε = 11 800 cm^{-1} M^{-1}) peak at 788 nm and a shoulder at 700 nm. On the basis of the intensity of the absorption (ε > 8000 M^{-1} cm^{-1}), we assign these strong transitions as ligand to metal charge transfer (LMCT) semiquinonate → V(dπ) excitations.[25,43,91−93]

The aqueous solution (pH = 3.36) of V^{IV}−hydroquinonate complex **2** shows only a very broad low-intensity peak that covers the middle visible region and gives the greenish-brown color to the complex. The decrease of the pH of the above solution down to 2.84 resulted in the immediate color change to deep blue, indicating the very fast oxidation of the hydroquinonate complex to semiquinonate from the atmospheric oxygen (Figure 6). The visible spectra of this solution

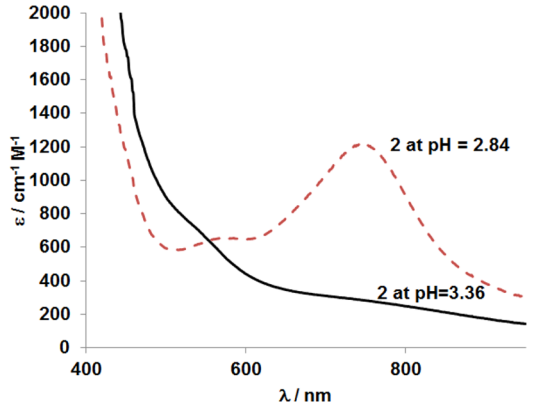

Figure 6. Absorption spectra of **2** at pH 3.36 and 2.84. The change of the spectrum is due to oxidation of **2** to **1** at lower pH.

show the appearance of a strong intensity peak at 750 nm and a shoulder at 570 nm assigned to the LMCT transitions of the semiquinonate complex. Although the structure of the semiquinonate complexes in aqueous and CH_3CN solutions is the same, the intensity of the charge transfer peak in H_2O is lower than the intensity in CH_3CN, indicating partial formation of the V^{IV}−semiquinonate complex in H_2O. A further decrease of the pH to 2.15 results in slow precipitation of the hexanuclear complex **5** and a decrease of the intensity of the peak at 750 nm. The rate of formation of **5** obeys second-order V^{IV}−semiquinonate complex-dependent kinetics with $t_{1/2}$ = 73 ± 1 min (Figure S4, Supporting Information).

Note that the formation of **4** from the semiquinonate complex **1** involves the replacement of the chlorine with the bridged oxygen donor atoms and electron transfer from the V^{IV} atoms to the semiquinonate ligand, resulting in the oxidation of V^{IV} to V^{V} and the reduction of semiquinonate ligand to hydroquinonate. Apparently, the oxophilicity of vanadium ions was increased at a lower pH. The electron transfer occurs at pH ≈ 2.2, which is close to the pK_a value of the ligand.[43,94,95]

Electrochemistry. The redox properties of the ligand and complexes **1** and **2** were investigated by cyclic voltammetry (CV) and rotating disk voltammetry (RD) in aqueous and CH_3CN solutions. The CVs of **1** and H_2bpymah in CH_3CN are shown in Figure 7, and the data are collected in Table 6. The

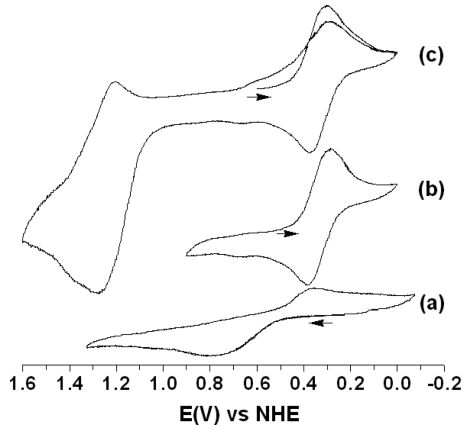

Figure 7. Cyclic voltamograms of H_2bbpymah ligand (a) and **1** (b and c) acquired in acetonitrile solvent (0.5 M $NBuClO_4$, N_2, 25 °C, 100 mV/s). Arrows indicate the initial potential scan.

Table 6. Electrochemical Data of H_2bpymah and 1 in Acetonitrile

compound	E_{pc} (V)	E_{pa} (V)	ΔE (mV)	$E_{1/2}$ (V)	assignment[a]
H_2bpymah	−0.82	−0.53	290		py reduction
	+0.35	+0.79	440		HQ → Q
1	−0.74	−0.53	290		py reduction
	+0.31	+0.38	75	+ 0.34	HQ → SQ
	+1.22	+1.28	60	+ 1.25	SQ → Q
		+1.40			V^{IV} → V^{V}

[a]py, denotes oxidation of pyridyl side arms of L1; HQ → Q, denotes oxidation of hydroquinone to quinone; HQ → SQ, denotes oxidation of hydroquinone to semiquinone; SQ → Q, denotes oxidation of semiquinone to quinone; V^{IV} → V^{V}, denotes oxidation of one of the V^{IV} to V^{V}.

free ligand in CH_3CN gave a single two-electron irreversible wave at $E_{1/2}$ = 0.57 V vs NHE (E_{pc} − E_{pa} = 440 mV) assigned to the oxidation of hydroquinone to quinone and the reverse. In CH_3CN, **1** and **2** gave cyclic voltammograms of the same shape exhibiting one reversible one-electron peak at $E_{1/2}$ = +0.34 V vs NHE (ΔE_p = 75 mV) assigned to the reduction of semiquinone ligand to hydroquinone for complex **1** or the oxidation of hydroquinone to semiquinone for complex **2**. In addition, at E ≈ 1.28 and 1.40 V vs NHE, two overlapped one-electron peaks were recorded, assigned to the oxidation of semiquinone to quinone and to the oxidation of one of the V^{IV} to V^{V}, respectively (Figure 7c). For electrochemically reversible

DOI: 10.1021/acs.inorgchem.5b00571
Inorg. Chem. 2015, 54, 7218−7229

processes, the plots of E versus $RT\ln[(i_d - i)/i]/F$ (F, Faraday's constant; R, gas constant) of the RDE voltammograms over a potential range between the quartile ($E_{1/4}$) and the three-quartile ($E_{3/4}$) potential values will be linear with an intercept of $E_{1/2}$ and slope $1/n$ (n, number of electrons).[96] The peak at 0.34 V meets these requirements with n equal to 1 for rotation speeds of 300, 500, and 1000 rpm. In addition, the $E_{1/2}$ value is essentially independent of the rotation speed, supporting the reversibility of the peak. The large difference between the semiquinone/hydroquinone and quinone/semiquinone redox couples (910 mV) indicates a large thermodynamic stabilization of the semiquinone radical in the complex.

Activity of the V^{IV}–Hydroquinonate/Semiquinonate Complexes Toward the O_2 Reduction. Oxidation of an aqueous or moist CH_3CN solution of **2** to **1** by O_2 results in the formation of H_2O_2. To trap any formed H_2O_2, NaV^VO_3 or $V^{IV}OCl_2$ was added in a D_2O solution of **2** before pH adjustment. The peroxide generated in solution primarily oxidizes VO^{2+} to vanadate. The vanadates react with peroxide and form peroxovanadates detected by ^{51}V NMR spectroscopy at −620 ppm (Figure S5, Supporting Information). An analogous experiment was conducted in CD_3CN, giving a peak at −355 ppm assigned to monoperoxovanadates (Figure 8). The ^{51}V NMR spectra of the CD_3CN solution of $VOCl_2$

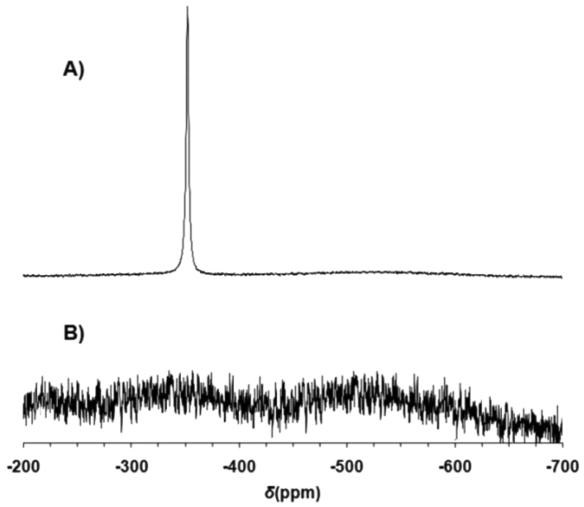

Figure 8. ^{51}V NMR spectrum of a (a) CD_3CN solution containing complex **2** (20 mM) and $VOCl_2$ (10 mM) after O_2 gas bubbling. (b) CD_3CN solution containing $VOCl_2$ (10 mM) after O_2 gas bubbling (blank sample). A chemical shift at −355 ppm was assigned to the monoperoxovanadate species.[97]

reacted with H_2O_2 gave a peak in a similar chemical shift. Addition of H_2O in the CD_3CN solution of peroxide induces a sharp shift (∼−120 ppm) to higher field, similar to the shift observed for the peroxo species in CD_3CN by Pecoraro's group, supporting our assigment.[97] The conditions of our experiment are more acidic than those previously reported experiments justifying the higher field observed chemical shift (∼75 ppm) in CD_3CN. It is important to note that the reactivity of the complex toward the production of H_2O_2 is highest in CD_3CN, most likely due to a better yield of the oxidation of **2** in CD_3CN than in D_2O (see above). Overall, the stoichiometries of the oxidation of $[\{V^{IV}(O)(Cl)\}_2(\mu\text{-bpymah})]$ and the pH-induced electron transfer reactions are shown in eqs 4 and 5

$$O_2 + 2H_2O + 2[\{V^{IV}(O)(Cl)\}_2(\mu\text{-bpymah})] \rightarrow 2[\{V^{IV}(O)(Cl)\}_2(\mu\text{-bpymas})] + OH^- + H_2O_2 \quad (4)$$

$$3[\{V^{IV}(O)(Cl)\}_2(\mu\text{-bpymas})]^+OH^- \rightleftharpoons [\{V^V(O)(\mu\text{-}O)V^{IV}(O)\}(\mu\text{-bpymah})]_3 + 3HCl \quad (5)$$

Direct oxidation of the hydroquinone ligand from dioxygen is not favored because of the low, one-electron, reduction potential of O_2 ($O_2 + H^+ + e^- \rightarrow HOO^{\bullet -}$; $E_0 = 0.12$ V) and due to spin restrictions.

Apparently, O_2 is activated by the transition metal. Coordination of O_2 to the metal ions results in an increase of the O_2 one-electron reduction potential and makes it kinetically more reactive.[98] Thus, a probable pathway will involve the interaction of O_2 with V^{IV} and then oxidation of the hydroquinone to semiquinone. An alternative mechanism proposed for the V^V–catecholate, *o*-semiquinonate complexes proceeds[99] through activation of the ligand by one-electron oxidation from the metal ion. However, this pathway should be less probable because the V^{IV} in the hydroquinonate complex **2** is a weak oxidant and incapable of oxidizing the ligand, as evident by its electrochemistry.

CONCLUSIONS

In this study, we presented the complete characterization of the first stable dinuclear V^{IV} σ-bonded *p*-semiquinonate complex synthesized from the aerial oxidation of a carefully designed V^{IV}–hydroquinonate radical trap. The V^{IV} ions of the semiquinonate complexes exhibit a surprisingly low oxophilicity, which leads to the unexpected stabilization of OH^- in acidic solutions and their cocrystallization as counterions for the **1** compound. At lower pH values, the semiquinonate complex is converted to the hexanuclear V^{IV}–O–V^V mixed-valent hydroquinonate complex because of an intramolecular metal to ligand proton-induced electron transfer. Magnetic measurements distinguish the hydroquinonate from the semiquinonate species and indicate that the spins in the dinuclear hydroquinonate and semiquinonate V^{IV} species are antifferomagnetically coupled. The one-electron ligand-centered redox reaction is reversible, as evidenced by cyclic voltammetry. Further investigation of the oxidation mechanism of these molecules is currently in progress.

ASSOCIATED CONTENT

Supporting Information

M vs H graph of **2**; X-band EPR spectra of an CH_3CN solution of **1**; ^{51}V NMR and ^1H NMR of DMSO-d_6 solution of **3** and assignments; UV–vis electronic spectra; ^{51}V NMR spectrum of an aqueous solution at pH 2.80 containing complex **2** (12.5 mM), $NaVO_3$ (6.25 mM) after O_2 gas bubbling; selected bond lengths and angles for **3** and **4**; molecular conductivity measurements for **1**–**4**. The Supporting Information is available free of charge on the ACS Publications website at DOI: 10.1021/acs.inorgchem.5b00571.

AUTHOR INFORMATION

Corresponding Author

*E-mail: akeramid@ucy.ac.cy.

Notes

The authors declare no competing financial interest.

DOI: 10.1021/acs.inorgchem.5b00571
Inorg. Chem. 2015, 54, 7218–7229

■ ACKNOWLEDGMENTS

We thank the Research Promotion Foundation of Cyprus for financial support of this work with proposals ENTAX/0505/14 and ENTAX/0504/8. We also thank the Research Promotional Foundation of Cyprus and the European Structural Funds for financial support of this work through ΑΝΑΒΑΘΜΙΣΗ/ΠΑΓΙΟ/0308/32.

■ REFERENCES

(1) Saito, K.; Rutherford, A. W.; Ishikita, H. *Proc. Natl. Acad. Sci. U.S.A.* **2013**, *110*, 954−959.
(2) Rappoport, Z. *The Chemistry of the Quinoid Compounds*; Wiley: New York, 1988; Vols. *1* and 2.
(3) Yano, T.; Magnitsky, S.; Ohnishi, T. *Biochim. Biophys. Acta, Bioenerg.* **2000**, *1459*, 299−304.
(4) Warren, J. J.; Tronic, T. A.; Mayer, J. M. *Chem. Rev.* **2010**, *110*, 6961−7001.
(5) Mure, M. *Acc. Chem. Res.* **2004**, *37*, 131−139.
(6) Johnson, B. J.; Yukl, E. T.; Klema, V. J.; Klinman, J. P.; Wilmot, C. M. *J. Biol. Chem.* **2013**, *288*, 28409−28417.
(7) Klema, V. J.; Wilmot, C. M. *Int. J. Mol. Sci.* **2012**, *13*, 5375−5405.
(8) Liu, Y.; Mukherjee, A.; Nahumi, N.; Ozbil, M.; Brown, D.; Angeles-Boza, A. M.; Dooley, D. M.; Prabhakar, R.; Roth, J. P. *J. Phys. Chem. B* **2013**, *117*, 218−229.
(9) Murakawa, T.; Hayashi, H.; Sunami, T.; Kurihara, K.; Tamada, T.; Kuroki, R.; Suzuki, M.; Tanizawa, K.; Okajima, T. *Acta Crystallogr., Sect. D: Biol. Crystallogr.* **2013**, *69*, 2483−2494.
(10) Baum, A. E.; Park, H.; Lindeman, S. V.; Fiedler, A. T. *Inorg. Chem.* **2014**, *53*, 12240−12242.
(11) Roy, A. S.; Saha, P.; Adhikary, N. D.; Ghosh, P. *Inorg. Chem.* **2011**, *50*, 2488−2500.
(12) Kundu, S.; Maity, S.; Maity, A. N.; Ke, S. C.; Ghosh, P. *Dalton Trans.* **2013**, *42*, 4586−4601.
(13) Sheriff, T.; Carr, P.; Piggott, B. *Inorg. Chim. Acta* **2003**, *348*, 115−122.
(14) Lewis, E. A.; Tolman, W. B. *Chem. Rev.* **2004**, *104*, 1047−1076.
(15) Rolle, C. J., III; Hardcastle, K. I.; Soper, J. D. *Inorg. Chem.* **2008**, *47*, 1892−1894.
(16) Hage, R.; Lienke, A. *Angew. Chem., Int. Ed.* **2006**, *45*, 206−222.
(17) Campos-Martin, J. M.; Blanco-Brieva, G.; Fierro, J. L. G. *Angew. Chem., Int. Ed.* **2006**, *45*, 6962−6984.
(18) Disselkamp, R. S. *Appl. Energy* **2011**, *88*, 4214−4217.
(19) Zhang, Y. G.; Pang, A. M.; Xiao, J. W.; Li, W. B.; Yuan, H.; Zeng, D. W. A novel kind of green high energy solid propellant containing hydrogen peroxide. *Proceedings of the International Astronautical Congress*; IAC: Beijing, China, 2013; pp 7010−7016.
(20) Liu, Z.; Sadler, P. J. *Acc. Chem. Res.* **2014**, *47*, 1174−1185.
(21) Santini, C.; Pellei, M.; Gandin, V.; Porchia, M.; Tisato, F.; Marzano, C. *Chem. Rev.* **2014**, *114*, 815−862.
(22) Lenaz, G. *Adv. Exp. Med. Biol.* **2012**, *942*, 93−136.
(23) Rehder, D. *Coord. Chem. Rev.* **1999**, *182*, 297−322.
(24) Rehder, D. *Bioinorganic Vanadium Chemistry*; John Wiley & Sons, Ltd.: New York, 2008.
(25) Cornman, C. R.; Colpas, G. J.; Hoeschele, J. D.; Kampf, J.; Pecoraro, V. L. *J. Am. Chem. Soc.* **1992**, *114*, 9925−9933.
(26) Cornman, C. R.; Kampf, J.; Soo Lah, M.; Pecoraro, V. L. *Inorg. Chem.* **1992**, *31*, 2035−2043.
(27) Schneider, C. J.; Penner-Hahn, J. E.; Pecoraro, V. L. *J. Am. Chem. Soc.* **2008**, *130*, 2712−2713.
(28) Hirao, T. *Chem. Rev.* **1997**, *97*, 2707−2724.
(29) Hanson, S. K.; Baker, T. R.; Gordon, J. C.; Scott, B. L.; L, T. D. *Inorg. Chem.* **2010**, *49*, 5611−5618.
(30) Spikes, G. H.; Sproules, S.; Bill, E.; Weyhermuller, T.; Wieghardt, K. *Inorg. Chem.* **2008**, *47*, 10935−10944.
(31) Mukherjee, C.; Weyhermuller, T.; Bothe, E.; P, C. *Inorg. Chem.* **2008**, *47*, 11620−11632.
(32) Chang, C. J.; Labinger, J. A.; Gray, H. B. *Inorg. Chem.* **1997**, *36*, 5927−5930.
(33) Chatterjee, P. B.; Bhattacharya, K.; Kundu, N.; Choi, K.-Y.; Clrac, R.; Chaudhury, M. *Inorg. Chem.* **2009**, *48*, 804−806.
(34) Conte, V.; Floris, B. *Dalton Trans.* **2011**, *40*, 1419−1436.
(35) Colpas, G. J.; Hamstra, B. J.; Kampf, J. W.; Pecoraro, V. L. *J. Am. Chem. Soc.* **1996**, *118*, 3469−3478.
(36) Ligtenbarg, A. G. L.; Hage, R.; Feringa, B. L. *Coord. Chem. Rev.* **2003**, *237*, 89−101.
(37) Crans, D. C.; Zhang, B.; Gaidamauskas, E.; Keramidas, A. D.; Willsky, G. R.; Roberts, C. R. *Inorg. Chem.* **2010**, *49*, 4245−4256.
(38) Sutradhar, M.; Shvydkiy, N. V.; Guedes Da Silva, M. F. C.; Kirillova, M. V.; Kozlov, Y. N.; Pombeiro, A. J. L.; Shul'Pin, G. B. *Dalton Trans.* **2013**, *42*, 11791−11803.
(39) Da Silva, J. A. L.; Fraústo da Silva, J. J. R.; Pombeiro, A. J. L. *Coord. Chem. Rev.* **2013**, *257*, 2388−2400.
(40) Kosugi, M.; Hikichi, S.; Akita, M.; Moro-oka, Y. *J. Chem. Soc., Dalton Trans.* **1999**, 1369−1371.
(41) Waidmann, C. R.; Dipasquale, A. G.; Mayer, J. M. *Inorg. Chem.* **2010**, *49*, 2383−2391.
(42) Drouza, C.; Keramidas, A. D. In *Charge distribution in vanadium p-(hydro/semi)quinonate complexes*; Kustin, K., Pessoa, J. C., Crans, D. C., Eds.; ACS Symposium Series, American Chemical Society: Washington, DC, 2007; Vol. *974*, pp 352−363.
(43) Drouza, C.; Keramidas, A. D. *Inorg. Chem.* **2008**, *47*, 7211−7224.
(44) Drouza, C.; Tolis, V.; Gramlich, V.; Raptopoulou, C.; Terzis, A.; Sigalas, M. P.; Kabanos, T. A.; Keramidas, A. D. *Chem. Commun.* **2002**, 2786−2787.
(45) Drouza, C.; Vlasiou, M.; Keramidas, A. D. *Dalton Trans.* **2013**, *42*, 11831−11840.
(46) Stylianou, M.; Drouza, C.; Viskadourakis, Z.; Giapintzakis, J.; Keramidas, A. D. *Dalton Trans.* **2008**, 6188−6204.
(47) Drouza, C.; Stylianou, M.; Papaphilippou, P.; Keramidas, A. D. *Pure Appl. Chem.* **2013**, *85*, 329−342.
(48) Keramidas, A. D.; Drouza, C.; Stylianou, M. σ-bonded *p*-Dioxalene Transision Metal Complexes. In *Current Trends in Cryrstallography*; Chandrasekaran, A., Ed.; INTECH: Croatia, 2011; pp 137−160.
(49) Drouza, C.; Keramidas, A. D. *J. Inorg. Biochem.* **2000**, *80*, 75−80.
(50) Vlasiou, M.; Drouza, C.; Kambanos, T. A.; Keramidas, A. D. *J. Inorg. Biochem.* **2015**, *147*, 39−43.
(51) Paul, R. C.; Bhatia, S.; Kumar, A.; Mague, J. T.; Weston, C. W. Vanadyl(IV) Acetate, $VO(CH_3CO_2)_2$. *Inorganic Synthesis*; John Wiley & Sons, Inc.: *New York*, 2007; pp 181−183.
(52) *CrysAlis CCD*, 1.171.29.9; Oxford Diffraction Ltd.: Abingdon, England, 2006.
(53) *CrysAlis RED*, 1.171.29.9; Oxford Diffraction Ltd.: Abingdon, England, 2006.
(54) Sheldrick, G. M. *SHELXL-97: Program for the Refinement of Crystal Structure*; University of Göttingen: Göttingen, Germany, 1997.
(55) Sheldrick, G. M. *SHELXS-97: Program for the Solution of Crystal Structure*; University of Göttingen: Göttingen, Germany, 1997.
(56) Farrugia, L. J. *J. Appl. Crystallogr.* **1999**, *32*, 837.
(57) Dutta, S. K.; Samanta, S.; Kumar, S. B.; Han, O. H.; Burckel, P.; Pinkerton, A. A.; Chaudhury, M. *Inorg. Chem.* **1999**, *38*, 1982−1988.
(58) Dutta, S. K.; Kumar, S. B.; Bhattacharyya, S.; Tienink, E. R. T.; Chaudhury, M. *Inorg. Chem.* **1997**, *36*, 4954−4960.
(59) Schmidt, H.; Bashirpoor, M.; Rehder, D. *J. Chem. Soc., Dalton Trans.* **1996**, 3865−3870.
(60) Dutta, S.; Basu, P.; Chakravorty, A. *Inorg. Chem.* **1993**, *32*, 5343−5348.
(61) Schulz, D.; Weyhermuller, T.; Wieghardt, K.; Nuber, B. *Inorg. Chim. Acta* **1995**, *240*, 217−229.
(62) Sarkar, A.; Pal, S. *Eur. J. Inorg. Chem.* **2009**, *2009*, 5391−5398.
(63) Mondal, S.; Ghosh, P.; Chakravorty, A. *Inorg. Chem.* **1997**, *36*, 59−63.
(64) Mahroof-Tahir, M.; Keramidas, A. D.; Goldfarb, R. B.; Anderson, O. P.; Miller, M. M.; Crans, D. C. *Inorg. Chem.* **1997**, *36*, 1657−1668.

DOI: 10.1021/acs.inorgchem.5b00571
Inorg. Chem. 2015, 54, 7218−7229

(65) Kojima, A.; Okazaki, K.; Ooi, S.; Saito, K. *Inorg. Chem.* **1983**, *22*, 1168−1174.
(66) Nishizawa, M.; Hirotsu, K.; Ooi, S.; Saito, K. *J. Chem. Soc., Chem. Commun.* **1979**, 707−708.
(67) Launay, J.-P.; Jeanin, Y.; Daoudi, M. *Inorg. Chem.* **1985**, *24*, 1052−1059.
(68) Holwerda, R. A.; Whittlesey, B. R.; Nilges, M. J. *Inorg. Chem.* **1998**, *37*, 64−68.
(69) Nikolakis, V. A.; Tsalavoutis, J. T.; Stylianou, M.; Evgeniou, E.; Jakusch, T.; Melman, A.; Sigalas, M. P.; Kiss, T.; Keramidas, A. D.; Kabanos, T. A. *Inorg. Chem.* **2008**, *47*, 11698−11710.
(70) Pierpont, C. G. *Inorg. Chem.* **2001**, *40*, 5727−5728.
(71) Pierpont, C. G.; Lange, C. W. *Nachr. Chem., Tech. Lab.* **1993**, *41*, 331−442.
(72) Gutlich, P.; Dei, A. *Angew. Chem., Int. Ed. Engl.* **1997**, *36*, 2734−2736.
(73) Adams, D. M.; Dei, A.; Rheingold, A. L.; Hendrickson, D. N. *J. Am. Chem. Soc.* **1993**, *115*, 8221−8229.
(74) Foster, C. L.; Liu, X.; Kilner, C. A.; Thornton-Pett, M.; Halcrow, M. A. *J. Chem. Soc., Dalton Trans.* **2000**, 4563−4568.
(75) Kunzel, A.; Sokolow, M.; Liu, F.; Roesky, H. W.; Noltemeyer, M.; Schmidt, H.; Uson, I. *J. Chem. Soc., Dalton Trans.* **1996**, 913−919.
(76) McQuillan, F. S.; Berridge, T. E.; Chen, H.; Hamor, T. A.; Jones, C. J. *Inorg. Chem.* **1998**, *37*, 4959−4970.
(77) Calderazzo, F.; Englert, U.; Pampaloni, G.; Passarelli, V. *J. Chem. Soc., Dalton Trans.* **2001**, 2891−2898.
(78) Sembiring, S.; Colbran, S. B.; Craig, D. C. *J. Chem. Soc., Dalton Trans.* **1999**, 1543−1554.
(79) Chun, H.; Chaudhuri, P.; Weyhermuller, T.; Wieghardt, K. *Inorg. Chem.* **2002**, *41*, 790−795.
(80) Carugo, O.; Castellani, C. B.; Djinovic, K.; Rizzi, M. J. *J. Chem. Soc., Dalton Trans.* **1992**, 837−841.
(81) Oswald, I. D. H.; Motherwell, W. D. S.; Parsons, S. *Acta Crystallogr., Sect. E: Struct. Rep. Online* **2004**, *60*, o1967−o1969.
(82) Arulsamy, N.; Bohie, D. S.; Butikofer, J. L.; Stephens, P. W.; Yee, G. T. *Chem. Commun.* **2004**, 1856−1857.
(83) Patil, A. O.; Curtin, D. Y.; Paul, I. C. *J. Am. Chem. Soc.* **1984**, *106*, 4010−4015.
(84) Pennington, W. T.; Patil, A. O.; Curtin, D. Y.; Paul, I. C. *J. Chem. Soc., Perkin Trans. 2* **1986**, 1693−1700.
(85) Wallwork, S. C.; Powell, H. M. *J. Chem. Soc., Perkin Trans. 2* **1980**, 641−646.
(86) Bolte, M.; Margraf, G.; Lerner, W. *Cambridge Crystallographic Database*; Cambridge Crystallographic Data Centre: Cambridge, UK, 2002.
(87) Sugiura, K.; Toyado, J.; Okamoto, H.; Okaniwa, K.; Mitani, T.; Kawamoto, A.; Tanaka, J.; Nakasuji, K. *Angew. Chem., Int. Ed. Engl.* **1992**, *31*, 852−854.
(88) Drouza, C.; Vlasiou, M.; Keramidas, A. D. *Inorg. Chim. Acta* **2014**, *420*, 103−111.
(89) Ricci, J. S.; Stevens, R. C.; McMullan, R. K.; Klooster, W. T. *Acta Crystallogr., Sect. B: Struct. Sci.* **2005**, *61*, 381−386.
(90) Drouza, C.; Stylianou, M.; Keramidas, A. D. *Pure Appl. Chem.* **2009**, *81*, 1313−1321.
(91) Hawkins, C. J.; Kabanos, T. A. *Inorg. Chem.* **1989**, *28*, 1084−1087.
(92) Bulls, A. R.; Pippin, C. G.; Hahn, F. E.; Raymond, K. N. *J. Am. Chem. Soc.* **1990**, *112*, 2627−2632.
(93) Cass, M. E.; Greene, D. L.; Buchanan, R. M.; Pierpont, C. G. *J. Am. Chem. Soc.* **1983**, *105*, 2680−2686.
(94) Baruah, B.; Das, S.; Chakravorty, A. *Inorg. Chem.* **2002**, *41*, 4502−4508.
(95) Rath, S. P.; Rajak, K. K.; Chakravorty, A. *Inorg. Chem.* **1999**, *38*, 4376−4377.
(96) Bard, A. J.; Faulkner, L. R. *Electrochemical Methods, Fundamentals and Applications*; Wiley: New York, 1980; pp (a) 160, 290; (b) 288; (c) 229.
(97) Slebodnick, C.; Pecoraro, V. L. *Inorg. Chim. Acta* **1998**, *283*, 37−43.
(98) Bakac, A. *Inorg. Chem.* **2010**, *49*, 3584−3593.
(99) Morris, A. M.; Pierpont, C. G.; Finke, R. G. *Inorg. Chem.* **2009**, *48*, 3496−3498.

DOI: 10.1021/acs.inorgchem.5b00571
Inorg. Chem. 2015, 54, 7218−7229